The Astrophysical Journal, 844:58 (9pp), 2017 July 20 https://doi.org/10.3847/1538-4357/aa7a12

Constraints on a Proton Synchrotron Origin of VHE Gamma Rays from the Extended Jet of AP Librae

Partha Pratim Basumallick and Nayantara Gupta
Raman Research Institute, C. V. Raman Avenue, Sadashivanagar, Bangalore 560080, India; basuparth314@gmail.com
Received 2017 February 6; revised 2017 June 7; accepted 2017 June 15; published 2017 July 21

Abstract

The multiwavelength photon spectrum from the BL Lac object AP Librae extends from radio to TeV gamma rays. The X-ray to very high-energy gamma-ray emission from the extended jet of this source has been modeled with inverse Compton (IC) scattering of relativistic electrons off the cosmic microwave background (CMB) photons. The IC/CMB model requires the kpc-scale extended jet to be highly collimated with a bulk Lorentz factor close to 10. Here we discuss the possibility of a proton synchrotron origin of X-rays and gamma rays from the extended jet with a bulk Lorentz factor of 3. This scenario requires an extreme proton energy of 3.98×10^{21} eV and a high magnetic field of 1 mG of the extended jet with jet power $\sim 5 \times 10^{48}$ erg s^{-1} in particles and the magnetic field (which is more than 100 times the Eddington luminosity of AP Librae) to explain the very high-energy gamma-ray emission. Moreover, we have shown that X-ray emission from the extended jets of 3C 273 and PKS 0637-752 could be possible by proton synchrotron emission with jet power comparable to the Eddington luminosities.

Key words: BL Lacertae objects: individual (AP Librae) – galaxies: active – galaxies: general – galaxies: jets – gamma rays: galaxies

1. Introduction

AP Librae, a low-frequency peaked BL Lac object at a redshift of 0.0486 (Disney et al. 1974), has been observed in radio to TeV gamma rays by several detectors. In comparison with other extragalactic sources that have been detected in X-rays from their extended jets (e.g., 3C 279 and PKS 0637-752), AP Librae has the distinguishing feature of also being detected in very high-energy (VHE) gamma rays. As a consequence of this uniqueness in the spectral energy distribution (SED) of AP Librae, the approach to modeling it presents some very interesting opportunities for investigation, especially in view of the fact that the VHE region of the spectra cannot be specifically attributed to a particular region inside the source (central core/parsec-scale jet/extended jet).

The multiwavelength spectra from BL Lacs are usually well described by the synchrotron self-Compton (SSC) model. It is difficult to distinguish between core and jet emission from the multiwavelength data. The high-energy (HE) photons detected by *Fermi*-Large Area Telescope (LAT) in the 100 MeV–100 GeV energy range and the VHE photons detected by the High Energy Stereoscopic System (H. E. S. S.) above 100 GeV (Abramowski 2015) provide good statistics for detailed modeling of AP Librae. Although in 2013 the *Fermi*-LAT data did show a flare with a maximum flux 3.5 times above the quiescent state, no flare was indicated in the VHE gamma-ray data recorded by H.E. S.S. from AP Librae at that time. Due to poor angular resolution, it was not possible to ascertain the location of gamma-ray emission in this source.

The spectrum from AP Librae has been modeled by SSC and external Compton (EC; see Hervet et al. 2015; Sanchez et al. 2015). The extended jet of AP Librae has been observed in radio and X-ray frequencies. This 14 kpc long and 4.8 kpc wide jet with similar morphologies in radio and X-rays (Kaufmann et al. 2013) has been modeled by inverse Compton (IC) emission by cosmic microwave background (CMB) photons (Sanchez et al. 2015; Zacharias & Wagner 2016).

It is not possible to fit all the data from AP Librae with a simple one-zone SSC model. More complicated scenarios have been considered in previous works. Within a blob-in-jet SSC scenario, Hervet et al. (2015) introduced many components of IC emission. They added up the synchrotron and SSC photon fluxes from the blob and a parsec-scale jet, the EC photon flux from blob-jet and blob–broad-line region interactions, and the second-order SSC photon flux from the blob to get the observed flux. The combined jet power due to thermal and non-thermal particles and the magnetic field required in their model is comparable to the Eddington luminosity of AP Librae, which is 3.75×10^{46} erg s^{-1}.

A compact zone with a Lorentz bulk factor of 20 and an extended jet of 10 kpc radius and a Lorentz bulk factor of 8 are the two emission regions of AP Librae in the study by Sanchez et al. (2015). The VHE gamma rays are mostly produced by IC/CMB in the extended jet in their model.

In a more recent study, Zacharias & Wagner (2016) modeled the multiwavelength spectrum from AP Librae with three zones, a blob, a parsec-scale jet, and a kpc-scale extended jet. The authors considered the same value of the bulk Lorentz factor ($\Gamma = 10$) for all three zones. Also in this case, the jet power required was found to be comparable to the Eddington luminosity.

A lepto-hadronic model has been invoked for AP Librae (Petropoulou et al. 2016), where Bethe–Heitler interactions and photomeson production inside the blob have been suggested as the origin of GeV–TeV gamma rays. In this case, hour-scale variability is expected in the VHE gamma-ray data due to their compact production region. Moreover, the jet power required in this model is 10^{47}–10^{48} erg s^{-1}, 10–100 times higher than the Eddington luminosity. The authors considered two zones: a compact blob and a parsec-scale jet of Lorentz bulk factor 8. The larger the emission region, the lower the seed photon density; as a result, Bethe–Heitler pairs and photomesons are less likely to be produced inside the jet.

Proton synchrotron emission from the extended jets of flat-spectrum radio quasars (FSRQs) has been studied for Pictor A, 3C 120, 3C 273, and PKS 0637-752 by Aharonian (2002);

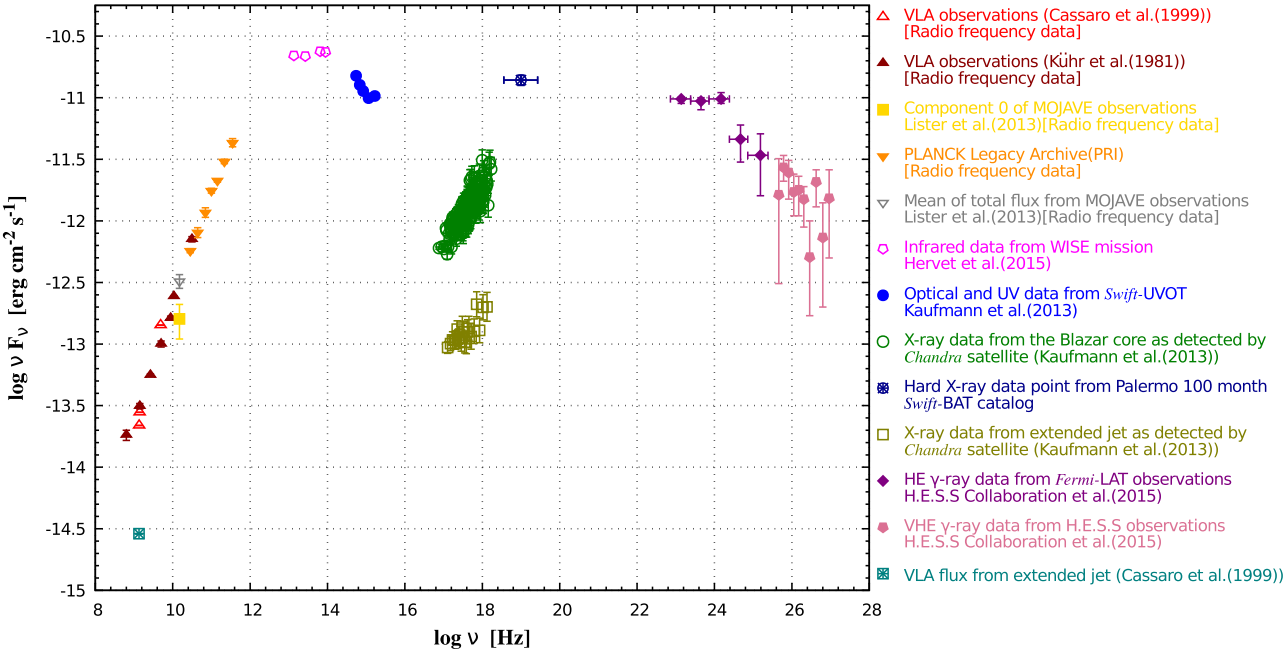

Figure 1. Quiescent-state multiwavelength emission spectra of AP Librae.

3C 273 by Kundu & Gupta (2014); and PKS 0637-752 by Bhattacharyya & Gupta (2016). The authors compared the synchrotron loss and escape timescales of the ultrahigh-energy protons with the age of the extended jet to determine the break energy in the proton spectrum and obtained the HE photon flux from the synchrotron emission of these trapped protons.

In the present work, the multiwavelength data compiled in Zacharias & Wagner (2016) have been used to study the possibility of a proton synchrotron origin of VHE gamma-ray emission from the extended jet of AP Librae. We have considered a three-zone model with a compact emission region or blob, a near parsec-scale jet, and an extended jet. In the next section, we discuss the spectra and radiation of relativistic electrons and protons in the compact region/blob near the core, the near parsec-scale jet, and the extended jet to explain the SEDs of AP Librae.

2. Modeling the SED

The multiwavelength data representing the quiescent state of AP Librae are presented in Figure 1. According to observations, all of the data points[1] in the radio frequency regime except the one at 1.36 GHz (Cassaro et al. 1999) are expected to originate from the central core region and parsec-scale jet of the source. The data point at 1.36 GHz depicted by the teal boxed asterisk (Figure 1) is attributed to the extended jet of AP Librae, as are the X-ray data points depicted by the olive green open squares. The green open circles, by contrast, are the X-ray frequency data that have the blazar core region as their source of origin. Both the core and the extended jet were detected in X-rays by the *Chandra* satellite and were reported by Kaufmann et al. (2013). The hard X-ray data point depicted by the navy blue circled asterisk was obtained from the Palermo 100 month *Swift*-Burst Alert Telescope (BAT) catalog. The infrared frequency data shown by the pink open pentagons are from the Wide-Field Infrared Survey Explorer (WISE) mission (Hervet et al. 2015), and the optical–UV frequency data depicted by the blue filled circles are from the *Swift*-Ultraviolet/Optical Telescope (UVOT) observations (Kaufmann et al. 2013).

We consider three separate emission regions to explain the observed spectra of AP Librae:

(i) a compact zone located near the blazar core, which we refer to as Zone-1 (Z1);
(ii) a region of near parsec-scale dimension, referred to as Zone-2 (Z2); and
(iii) an emission region in the extended jet of AP Librae, referred to as Zone-3 (Z3).

The observed data points in the radio–optical–UV frequency region are easily explained by the electron synchrotron emission from Zone-1 and Zone-2 and the radiation from the accretion disk of AP Librae. The X-ray frequency data depicted by the green open circles and olive green open squares are explained by SSC emission from Zone-1 and proton synchrotron emission from Zone-3, respectively. However, as the spatial resolution is comparatively poor for observations in the >100 MeV–to–TeV range, it is not possible to distinguish either region as the source for the data points in that energy range. By contrast, because the VHE gamma rays detected by H.E.S.S. (Abramowski 2015) show no evidence of variability (as of now), it makes for a possible argument in favor of prescribing the extended jet of AP Librae as the emission region for the HE–VHE portion of the observed SED. Although according to the reports of Abramowski (2015), AP Librae indicates variability on a scale of a few days above the energy of 300 MeV, it does not act as an essential factor in determining the emission region, as the present paper deals with the quiescent-state spectra of AP Librae. In any case, as the spectra in the HE–VHE gamma-ray region comprise both proton synchrotron emission from the extended jet and SSC emission from Zone-2 (whose dimensions are consistent with a variability timescale of a few days), our model should, in principle, account for the nonquiescent state of AP Librae as well. The HE and VHE gamma-ray data points are depicted by

[1] Red open triangles: Cassaro et al. (1999); maroon filled triangles: Kühr et al. (1981); yellow filled square: Lister et al. (2013); orange filled triangles: PLANCK Legacy Archive; gray open triangle: Lister et al. (2013).

the purple filled diamonds and pale pink filled pentagons, respectively. As it is expected that the data in the higher-energy regime of the SED should suffer from absorption due to the extragalactic background light (EBL), the presented data points have been corrected accordingly for the intergalactic absorption using the EBL model of Franceschini et al. (2008).

Although Sanchez et al. (2015) and Zacharias & Wagner (2016) considered the extended jet as the source of the HE and VHE emission of AP Librae, they relied on the IC emission mechanism to explain the higher-energy emission in the observed SED. The present work, by contrast, studies the possibility of proton synchrotron radiation from the extended jet of AP Librae to account for the HE–VHE gamma-ray emission while simultaneously explaining the X-ray data originating from the extended jet.

2.1. Particle Spectra in Zone-1 and Zone-2

The electron spectra in Zone-1 and Zone-2 are broken power laws, as they are cooling fast by SSC emission:

$$\frac{dN_{\rm el}(E_{\rm el})}{dE_{\rm el}} = A\begin{cases} E_{\rm el}^{-p_1} & E_{\rm el} < E_{\rm el}^{\rm brk} \\ E_{\rm el}^{\rm brk} E_{\rm el}^{-p_1-1} & E_{\rm el} > E_{\rm el}^{\rm brk}. \end{cases} \quad (1)$$

Out of the several input parameters required by the code, the extrema of the relativistic particles along with the so-called break energy $E_{\rm el}^{\rm brk}$ are a prime factor in determining the generated spectrum. The break energy is determined by equating the cooling time $t_{\rm cool}$ with $t_{\rm esc} = \eta_{\rm esc} \times \frac{R}{c}$, where $\frac{R}{c}$ is the light travel time in the emission region and $\eta_{\rm esc}$ acts as a scaling factor. The cooling timescale of the electrons is given by the expression

$$\frac{1}{t_{\rm cool}} = \frac{1}{t_{\rm synch}} + \frac{1}{t_{\rm SSC}}, \quad (2)$$

which is a convolution of both the synchrotron cooling and SSC cooling timescales of the electrons. In a more detailed form, Equation (2) can be expressed as

$$\frac{1}{t_{\rm cool}} = \frac{4}{3}\sigma_{\rm Th}^{\rm el}\beta_{\rm el}^2\gamma_{\rm el}\frac{c}{m_{\rm el}c^2}(U_B + U_{\rm el}^{\rm synch}), \quad (3)$$

where $\sigma_{\rm Th}^{\rm el}$ is the Thomson cross-section of electrons. The dimensionless speed of electrons $\beta_{\rm el} \simeq 1$, the Lorentz factor $\gamma_{\rm el} = \frac{E_{\rm el}}{m_{\rm el}c^2}$, and $U_B\left(=\frac{B^2}{8\pi}\right)$ and $U_{\rm el}^{\rm synch}$ are the energy densities[2] of the magnetic field and the synchrotron radiation generated by the electrons, respectively. Equation (3) is valid only for scatterings in the Thomson regime. The Klein–Nishina effect does not play a significant role in our calculations. In our model, the radius of the central core region is assumed to be $R_{Z1} = 8.65 \times 10^{16}$ cm, while the radius of the parsec-scale region is taken as $R_{Z2} = 9.5 \times 10^{17}$ cm. The magnetic fields in the two zones are $B_{Z1} = 8.5$ and $B_{Z2} = 1.72$ mG, respectively. The scaling factors $\eta_{\rm esc}$ for Zone-1 and Zone-2 are 62 and 63, respectively. As the value of $U_{\rm el}^{\rm synch}$ is sensitive to the magnetic field, energy range, and energy density of the particle population, we have to adjust our parameter values before we can fix the break energy of the electrons for a suitable choice of $\eta_{\rm esc}$. The relativistic protons are cooled by synchrotron emission inside the blob. The synchrotron emission from relativistic protons inside Zone-1 and Zone-2 is generated by assuming that the energy density ratio between protons and electrons is 1000:1. Proton cooling is not important in these zones, and, as the cooling timescale is long, no break appears in the proton spectrum. The maximum energy of the protons in the emission region is constrained by the condition

$$B \geqslant 30\frac{E_p^{\rm max}}{10^{19}}\frac{10^{15}}{R} \quad \text{in Gauss}, \quad (4)$$

which ensures that, for our choice of B, the Larmor radii of protons with energy $E_p^{\rm max}$ (in eV) do not exceed the chosen value of R. Miller et al. (1974) specifically reports the variability of 20 min, whereas (Webb et al. 1988; Carini et al. 1991) deal with the intraday scale variability (in the optical frequency regime) of AP Librae in general. However, according to the approximate relation

$$R \leqslant \frac{c\Delta t_{\rm obs}\delta}{1+z}, \quad (5)$$

a variability timescale ($\Delta t_{\rm obs}$) of 1 day for the Doppler factor $\delta = \frac{1}{\Gamma(1-\beta\cos\theta)} = 12.3$ gives the radius of the emission region as $\sim 3 \times 10^{16}$ cm. Similarly, for the *Fermi*-LAT observed 6 day variability in frequencies above 300 MeV, the radius of the emission region should be $\sim 2 \times 10^{17}$ cm. However, taking into account the fact that Equation (5) might lead to large errors while estimating the dimensions of the emitting region (Protheroe 2002), our estimate of $R_{Z1} = 8.65 \times 10^{16}$ and $R_{Z2} = 9.5 \times 10^{17}$ cm should be admissible even when modeling the optical frequency data with day/intraday scale variability and the HE gamma-ray frequency data with week scale variability.

2.2. Particle Spectra in Extended Jet

The electron spectrum in the extended jet (Zone-3) also follows a broken power law given by Equation (1). The electron population in the extended jet radiates primarily via synchrotron emission (unlike the blob, where SSC cooling is also a major contributor). The break energy of electrons $E_{\rm brk,jet}^{\rm el}$ is calculated by equating the synchrotron cooling time ($t_{\rm synch}^{\rm el}$) with the extended jet lifetime ($t_{\rm jet}$):

$$t_{\rm synch}^{\rm el} = t_{\rm jet} \Rightarrow \frac{\gamma_{\rm el}m_{\rm el}c^2}{\frac{4}{3}\sigma_{\rm Th}^{\rm el}cU_B\gamma_{\rm el}^2\beta_{\rm el}^2} = t_{\rm jet}. \quad (6)$$

The age of the extended jet $t_{\rm jet}$ is assumed to be of the order of 10^5–10^7 yr. We note that the justification for assuming this age is to allow the ultrahigh-energy protons to cool down by synchrotron emission during the lifetime of the jet.

The proton synchrotron emission from the extended jet of AP Librae is considered to be the origin of the HE–VHE gamma rays in our model. A broken power-law proton

[2] Throughout the paper, all the expressions and values of energy densities are in the comoving frame of the emission regions unless otherwise mentioned.

spectrum is required to fit the gamma-ray data:

$$\frac{dN_p(E_p)}{dE_p} = A\begin{cases} E_p^{-p_1} & E_p < E_p^{\rm brk} \\ E_p^{{\rm brk}(p_2-p_1)}E_p^{-p_2} & E_p > E_p^{\rm brk}. \end{cases} \quad (7)$$

We consider the energy-dependent diffusive escape of particles from the kpc-scale extended jet and not the much smaller Doppler-boosted compact regions because the particles escape from the compact regions at a much faster rate, implying no significant amount of diffusion.

We compare the synchrotron cooling time with the age of the extended jet and the escape timescale of the protons to fix the break energy. The resulting proton spectrum is characterized by a change in the spectral index from p_1 before the break to p_2 after the break, in Bohm diffusion limit $p_2 = p_1 + 1$. Also, as both electrons and protons are accelerated in the same region, whether it be the blob or the extended jet, the spectral indices for both particle populations (p_1) before cooling have been kept the same for the specific emission regions. The maximum energy of the protons, by contrast, is constrained by the condition in Equation (4). The minimum energy of the protons is a free parameter and set to values of the order of $\sim 10^{16}$–10^{17} eV. Although the minimum energy values are a consequence of the modeling requirements of the observed SED, higher values of minimum energy reduce the jet power appreciably.

The escape timescale and synchrotron cooling time of the protons are given by Equations (8) and (9), respectively.[3]

$$t_{\rm esc,Bohm} \simeq 4.2 \times 10^5 \eta^{-1} B_{\rm mG} R_{\rm kpc}^2 (E_p/10^{19}\ {\rm eV})^{-1}\ {\rm yr} \quad (8)$$

$$t_{\rm synch} \simeq 1.4 \times 10^7 B_{\rm mG}^{-2} (E_p/10^{19}\ {\rm eV})^{-1}\ {\rm yr}. \quad (9)$$

In Equation (8), η is the gyrofactor that assumes a value of 1 in the Bohm diffusion limit, $B_{\rm mG}$ is the ambient magnetic field (expressed in mG) in the extended jet, and $R_{\rm kpc} = \frac{R}{3.08 \times 10^{21}}$, where R is the radius of the emission zone (expressed in cm) in the extended jet. When modeling the data in the Bohm diffusion regime, we assume the value of $t_{\rm jet} = 2 \times 10^7$ yr. In our model in the Bohm diffusion regime, $E_p^{\rm brk} = 2.51 \times 10^{18}$ eV, for which the values of $t_{\rm esc}$ and $t_{\rm synch}$ are 2.53×10^7 and 5.6×10^7 yr, respectively, which are comparable to the extended jet lifetime of 2×10^7 yr.

We also consider the Kolmogorov and Kraichnan diffusion regimes to study the proton synchrotron model. The diffusion timescale is given as

$$t_{\rm esc} \simeq \frac{R}{c}\left(\frac{E_p}{E_{\rm free}}\right)^{-\alpha}, \quad (10)$$

where $E_{\rm free} = E^* B_4 R_{14}$, with $E^* = 3 \times 10^{20}$ eV, $B_4 = \frac{B}{10^4}$ G, and $R_{14} = \frac{R}{10^{14}}$ cm, and $\alpha = \frac{1}{3}$ and $\frac{3}{5}$ for the Kolmogorov and Kraichnan diffusion timescales. Spectral indices in the Kolmogorov model are $p_{1,\rm Kol}$ and $p_{2,\rm Kol} = p_{1,\rm Kol} + \frac{1}{3}$ and in the Kraichnan model are $p_{1,\rm Kra}$ and $p_{2,\rm Kra} = p_{1,\rm Kra} + \frac{3}{5}$. In the Kolmogorov diffusion regime, the escape timescale is 2.65×10^5 yr, whereas that in the Kraichnan diffusion regime is 2.1×10^6 yr. The break energy for the electron population is calculated assuming a jet lifetime of 2×10^5 and 2×10^6 yr for the Kolmogorov and Kraichnan diffusion regimes, respectively. The various values of the parameters used in the three diffusion regimes are presented in Table 1.

Although considering the different diffusive escape timescales does not affect the energetics, and the parameter values are also similar, it does serve the purpose of showing that, in spite of large variations in the escape timescales (which are compared with the jet lifetime to ascertain the break energy), the values of the other parameters are hardly affected. Moreover, as there are widely different estimates of the jet lifetime ($\sim 10^7$–10^8 yr, Aharonian 2002; and $\sim 10^5$ yr, Kusunose & Takahara 2017), the assumption of different diffusive escape timescales allows us to consider comparable estimates of the jet lifetime. The fact that similar parameter values are required for each case is only found as a result of our study.

If we assume an energy-independent escape of protons from the extended jet, then the escape time is $t_{\rm esc} = \eta_{\rm esc} \times \left(\frac{R}{c}\right)$. The break energy in the proton spectrum is determined in this case by equating the synchrotron timescale to the escape timescale. We find that this scenario requires a very high value of the scaling factor $\eta_{\rm esc} = 4409$, compared to the compact regions. It is worth noting in this context that assuming an energy-independent escape timescale does not require changing our parameter values for the proton synchrotron spectrum from the extended jet.

The value of the bulk Lorentz factor is assumed to be 7 in Zone-1 and Zone-2 and 3 for the extended jet labeled Zone-3. The corresponding values of the viewing angle $\theta_{\rm obs}$ are assumed to be 3° in Zone-1 and Zone-2 and 5°.5 in Zone-3. The values of the Doppler factor (δ) are 12.3 and 5.42 for the respective zones.

As mentioned earlier, the maximum energy of protons in the extended jet is 3.98×10^{21} eV. Hillas (1984), Cesarsky (1992), Rachen & Bierman (1993), and Henri et al. (1999) have discussed that the active galactic nuclei (AGNs) jets can act as potential sites for accelerating protons up to energies of 10^{20} eV. According to the findings of Ebisuzaki & Tajima (2014), intense electromagnetic fields may give rise to a plasma wakefield that can accelerate protons to energies beyond 10^{21} eV. The acceleration mechanism in such a case would then be credited to the Lorentz invariant ponderomotive force. For our choice of ambient magnetic field $B = 1$ mG, the emission region radius of $R = 1.2 \times 10^{22}$ cm is sufficient for accelerating the protons to 3.98×10^{21} eV from Equation (4). We note that although the maximum energy of the protons may be very high from the Hillas criterion, when considering known acceleration mechanisms it is difficult to explain such a high value (Aharonian et al. 2002). While selecting the radius ($R = 1.2 \times 10^{22}$ cm $= 3.9$ kpc) of the emission region, we have also considered the present estimates of the extended jet dimensions (length: 14 kpc; width: 4.8 kpc; Kaufmann et al. 2013).

The three-zone modeling of the observed SED of AP Librae is presented in Figure 2 (Bohm diffusion regime), Figure 3 (Kolmogorov diffusion regime), and Figure 4 (Kraichnan diffusion regime), along with the relevant parameters used while modeling the data in Table 1. The corresponding power requirement in the three zones is discussed in Section 3 along with the other findings (see Table 2).

The contributions of disk, broadline region (BLR), and torus radiation to the IC emission by the blob and pc-scale jet of AP Librae are considered in earlier papers. The energy of the BLR

[3] Refer to Aharonian (2002) for a detailed discussion.

Table 1
Parameters for Multiple-Zone Modeling of the Multiwavelength Data from the Quiescent-State Emission of AP Librae

Fitted SED	Region	Emission[a,b]	Γ	θ_{obs}	δ	B (mG)	R (cm)	E_{min} (eV)	E_{max} (eV)	E_{break} (eV)	p_1	p_2
Figure 2 Bohm diffusion regime	Zone-1	e^- synch+SSC	7	3°	12.3	8.5	8.65×10^{16}	3.55×10^{8}	6.31×10^{9}	5.64×10^{9}	2.15	3.15
		p^+ synch						3.16×10^{15}	2.45×10^{17}	…	2.15	…
	Zone-2	e^- synch+SSC	7	3°	12.3	1.72	9.5×10^{17}	2.24×10^{7}	3.55×10^{10}	3.51×10^{10}	1.9	2.9
		p^+ synch						3.16×10^{16}	5.45×10^{17}	…	1.9	…
	Zone-3	e^- synch	3	5°.5	5.42	1	1.2×10^{22}	6.31×10^{5}	3.98×10^{8}	6.5×10^{5}	1.87	2.87
		p^+ synch						6.31×10^{16}	3.98×10^{21}	2.51×10^{18}	1.87	2.87
Figure 3 Kolmogorov diffusion regime	Zone-1	e^- synch+SSC	7	3°	12.3	8.5	8.65×10^{16}	3.55×10^{8}	6.31×10^{9}	5.64×10^{9}	2.15	3.15
		p^+ synch						3.16×10^{15}	2.45×10^{17}	…	2.15	…
	Zone-2	e^- synch+SSC	7	3°	12.3	1.72	9.5×10^{17}	2.24×10^{7}	3.55×10^{10}	3.51×10^{10}	1.9	2.9
		p^+ synch						3.16×10^{16}	5.45×10^{17}	…	1.9	…
	Zone-3	e^- synch	3	5°.5	5.42	1	1.2×10^{22}	1.78×10^{6}	10^{9}	6.31×10^{7}	2.5	2.83
		p^+ synch						3.8×10^{17}	3.98×10^{21}	3.98×10^{17}	2.5	2.83
Figure 4 Kraichnan diffusion regime	Zone-1	e^- synch+SSC	7	3°	12.3	8.5	8.65×10^{16}	3.55×10^{8}	6.31×10^{9}	5.64×10^{9}	2.15	3.15
		p^+ synch						3.16×10^{15}	2.45×10^{17}	…	2.15	…
	Zone-2	e^- synch+SSC	7	3°	12.3	1.72	9.5×10^{17}	2.24×10^{7}	3.55×10^{10}	3.51×10^{10}	1.9	2.9
		p^+ synch						3.16×10^{16}	5.45×10^{17}	…	1.9	…
	Zone-3	e^- synch	3	5°.5	5.42	1	1.2×10^{22}	1.41×10^{6}	10^{9}	6.17×10^{6}	2.25	2.85
		p^+ synch						3.8×10^{17}	3.98×10^{21}	7.08×10^{17}	2.25	2.85

Notes. The different diffusion regimes are assumed for the emission from the extended jet.
[a] SSC emission from Zone-3 is found to be negligible.
[b] The proton synchrotron emission spectra from Zone-1 and Zone-2 follow a simple power law, whereas the proton synchrotron emission from Zone-3 follows a broken power-law spectrum with the spectral indices being defined by the three different diffusion regimes as mentioned earlier.

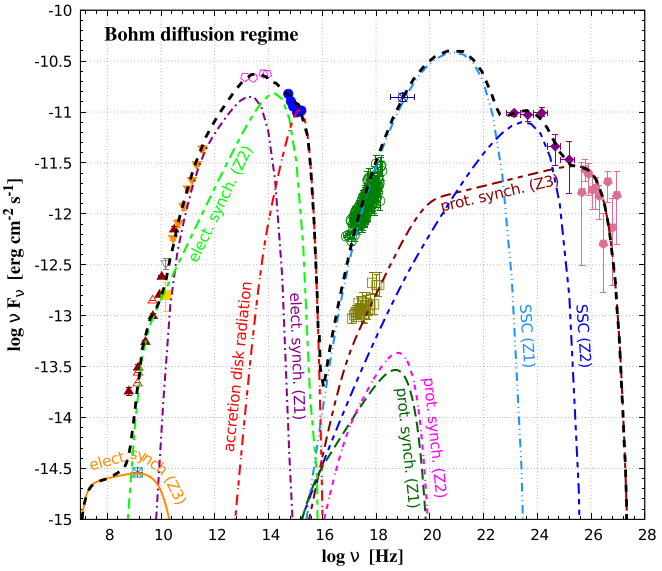

Figure 2. Multiple-zone modeling of the observed steady-state spectra of AP Librae for the Bohm diffusion regime. The purple dot-dashed line depicts the electron synchrotron emission from the compact blob designated as Zone-1. The lime green short-dashed long-dashed line depicts the electron synchrotron emission from the parsec-scale jet designated as Zone-2. The orange solid line depicts the electron synchrotron emission from the extended jet designated as Zone-3. The red dot-dashed line depicts the blackbody radiation from the accretion disk. The cyan double-dot-dashed line depicts the SSC emission from Zone-1. The dark green dashed line depicts the proton synchrotron emission from Zone-1. The dark blue double-short-dashed long-dashed line depicts the SSC emission from Zone-2. The magenta dot-double-dashed line depicts the proton synchrotron emission from Zone-2. The dark red double-short-dashed double-long-dashed line depicts the proton synchrotron emission from Zone-3. The black dashed line depicts the overall emission spectra of the quiescent-state multiwavelength data of AP Librae. The code developed by Krawczynski et al. (2004) is used to generate the spectra from different emission mechanisms.

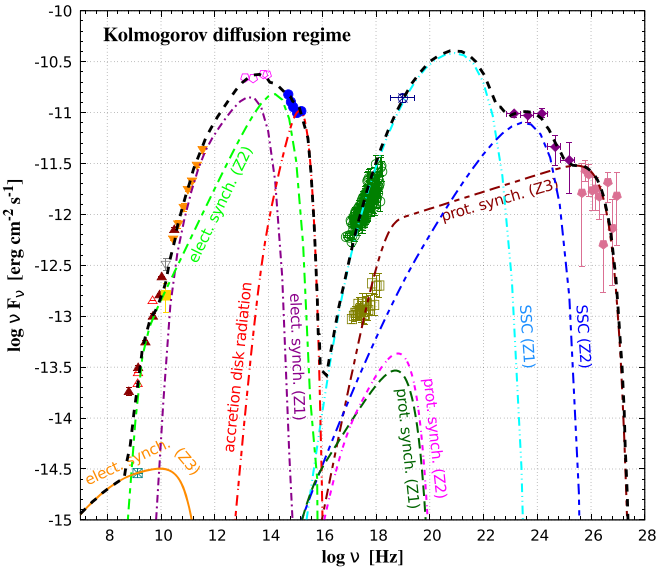

Figure 3. Same as Figure 2, but for the Kolmogorov diffusion regime.

photons is blueshifted in the rest frame of the blob. The reprocessed BLR emission has been parameterized in Equation (12) of Hervet et al. (2015). The parameter values presented in Table 3 of Hervet et al. (2015) have been chosen such that at HE, the EC emission of blob-BLR origin is significant. A similar discussion is given in Zacharias & Wagner (2016). Direct emissions from the disk, BLR, and torus are low as they

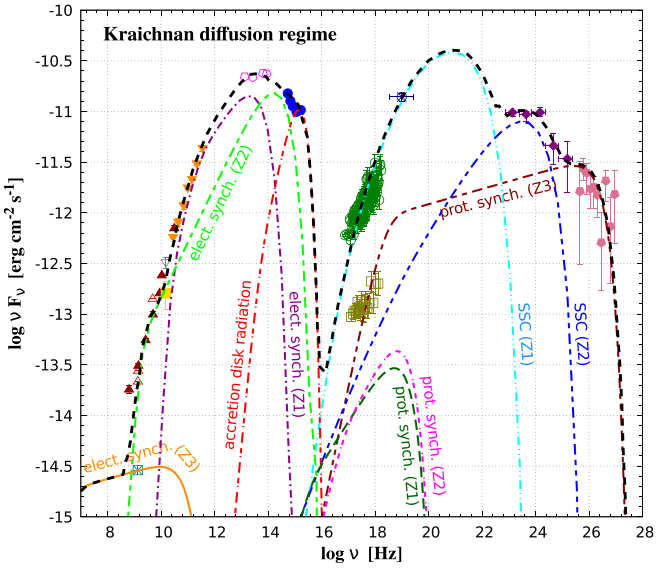

Figure 4. Same as Figure 2, but for the Kraichnan diffusion regime.

are not detected, however, EC emission from the blob due to the reprocessed emission could be significant (depending on the parameter values chosen and the distances of the blob and jet from the black hole) after Doppler boosting. Moreover, it is discussed that, due to the outward relativistic motion of the blob and its distance from the accretion disk, the EC emission of blob electrons due to disk radiation is negligible.

From Equation (A.6) of Zacharias & Wagner (2016), the energy density of reprocessed emission from the dusty torus in the reference frame of the blob is $u_{\rm DT} = \frac{4}{3}\Gamma^2 \frac{L_{\rm DT}\tau_{\rm DT}}{4\pi r_{\rm DT}^2 c}$. Assuming the radius of the region within which the emission is confined to be $r_{\rm DT} = 1$ pc, luminosity $L_{\rm DT} = 10^{42}$ erg s^{-1}, the Lorentz factor of the blob $\Gamma = 7$, the efficiency of reprocessing $\tau_{\rm DT} = 0.001$, and the energy density in radiation $u_{\rm DT} = 2 \times 10^{-8}$ erg cm^{-3}, which is much lower than the synchrotron photon energy density inside the blob, 1.28×10^{-5} erg cm^{-3}. By adjusting the parameter values suitably, the energy density in reprocessed external radiation could be made even lower. Moreover, the pc jet is assumed to be located beyond the BLR and torus region, which makes EC emission insignificant.

3. Results and Discussions

As shown in Figures 2–4, the observed quiescent-state SED of AP Librae has been fitted by the three-zone model adopted in the present work. The optical–UV frequency data in the SED are accounted for partially by the synchrotron emission of electrons from the blob and partially by the blackbody radiation from the accretion disk. The thermal emission from the accretion disk is reproduced by assuming a Shakura–Sunyaev type disk (Shakura & Sunyaev 1973) with a luminosity of $L_D = 1.3 \times 10^{44}$ erg s^{-1}. Incidentally, Zacharias & Wagner (2016) used the same estimate for disk luminosity,

$$P_{\rm jet} = \pi R^2 \Gamma^2 c (U_{\rm el} + U_{\rm pr} + U_B). \quad (11)$$

The jet power requirements from each region are calculated from the expression of $P_{\rm jet}$ presented in Equation (11). For the parameters used in our model, we find that the required jet power in Zone-1 is 5.7×10^{47} erg s^{-1} and in Zone-2 is $3.75 \times$

Table 2
Particle and Magnetic Energy Densities in Individual Zones along with Their Contribution to the Jet Power for Multiple-Zone Modeling of the Multiwavelength Data of Quiescent-State Emission from AP Librae

Fitted SED	Region	Particle	$u'_{\rm part.}$ erg cm^{-3}	$u'_B(=B^2/8\pi)$ erg cm^{-3}	R cm	Γ	$P'_{{\rm part.},Z}$ erg s^{-1}	$P'_{B,Z}$ erg s^{-1}	$P'_{{\rm total},Z}$ erg s^{-1}
Figure 2 Bohm diffusion regime	Zone-1	Electron	1.65×10^{-2}	2.87×10^{-6}	8.65×10^{16}	7	5.7×10^{44}	9.92×10^{40}	5.7×10^{47}
		Proton	1.65×10^{1}				5.7×10^{47}		
	Zone-2	Electron	9×10^{-5}	1.18×10^{-7}	9.5×10^{17}	7	3.75×10^{44}	4.9×10^{41}	3.75×10^{47}
		Proton	9×10^{-2}				3.75×10^{47}		
	Zone-3	Electron	1.9×10^{-15}	3.98×10^{-8}	1.2×10^{22}	3	2.32×10^{41}	4.85×10^{48}	4.86×10^{48}
		Proton	2.1×10^{-11}				2.56×10^{45}		
Figure 3 Kolmogorov diffusion regime	Zone-1	Electron	1.65×10^{-2}	2.87×10^{-6}	8.65×10^{16}	7	5.7×10^{44}	9.92×10^{40}	5.7×10^{47}
		Proton	1.65×10^{1}				5.7×10^{47}		
	Zone-2	Electron	9×10^{-5}	1.18×10^{-7}	9.5×10^{17}	7	3.75×10^{44}	4.9×10^{41}	3.75×10^{47}
		Proton	9×10^{-2}				3.75×10^{47}		
	Zone-3	Electron	3.1×10^{-16}	3.98×10^{-8}	1.2×10^{22}	3	3.78×10^{40}	4.85×10^{48}	4.86×10^{48}
		Proton	2.1×10^{-11}				2.56×10^{45}		
Figure 4 Kraichnan diffusion regime	Zone-1	Electron	1.65×10^{-2}	2.87×10^{-6}	8.65×10^{16}	7	5.7×10^{44}	9.92×10^{40}	5.7×10^{47}
		Proton	1.65×10^{1}				5.7×10^{47}		
	Zone-2	Electron	9×10^{-5}	1.18×10^{-7}	9.5×10^{17}	7	3.75×10^{44}	4.9×10^{41}	3.75×10^{47}
		Proton	9×10^{-2}				3.75×10^{47}		
	Zone-3	Electron	6.1×10^{-16}	3.98×10^{-8}	1.2×10^{22}	3	7.44×10^{40}	4.85×10^{48}	4.86×10^{48}
		Proton	2.1×10^{-11}				2.56×10^{45}		

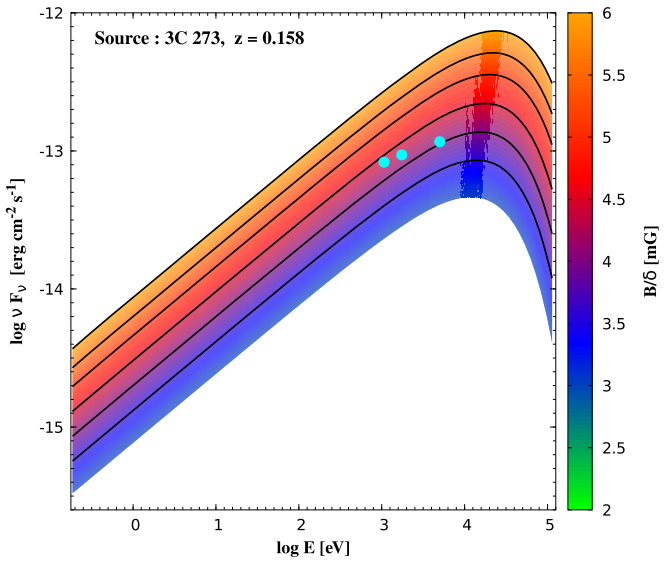

Figure 5. Photon flux from proton synchrotron emission vs. energy (in logscale) contour plot assuming equipartition of energy in protons and a magnetic field. The contour lines are for specific values of the magnetic field B, which is equivalent to $\frac{B}{\delta}$ (as $\delta = 1$ for these plots). The contour lines range from $\frac{B}{\delta} = 3.5$ to 6 mG in steps of 500 μG.

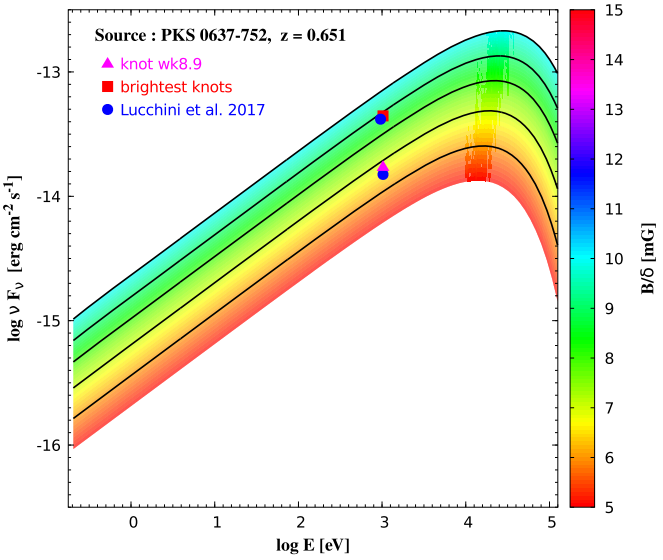

Figure 6. Same as Figure 5, but for the source PKS 0637-752. The contour lines range from $\frac{B}{\delta} = 6$ to 10 mG in steps of 1 mG. The blue points are taken from Lucchini et al. (2017).

10^{47} erg s^{-1}. The jet power requirement in Zone-3 is 4.86×10^{48} erg s^{-1}.

Assuming a simple power-law proton spectrum of spectral index 2 in the energy range of 10^{15}–10^{18} eV, we have calculated the photon fluxes for the extended jets of 3C 273, PKS 0637-752, and B3 0727+409 to explain the X-ray data with the proton synchrotron model. The emission region is assumed to be of radius 1 kpc, and its Doppler factor is fixed at 1 for simplicity. Figures 5–7 show the contour plots for the extended jets of these three sources for the magnetic field within 15 mG. We have also assumed equipartition in energy between the magnetic field and the relativistic protons. The jet power required to explain the observed X-ray data is $\sim 1.28 \times 10^{48}$ erg s^{-1} (corresponding to 4.25 mG) for 3C 273, $\sim 3 \times 10^{48}$ erg s^{-1} for knot wk8.9 (corresponding to 6.5 mG), and $\sim 5.75 \times 10^{48}$ erg s^{-1} for the brightest knot (corresponding to 9 mG) of PKS 0637-752. The Eddington luminosity of 3C 273 and PKS 0637-752 could be as high as 10^{48} erg s^{-1} (Paltani & Türler 2005, Kusunose & Takahara 2017). Thus, the jet power required to explain the X-ray data from the extended jets of 3C 273 (for a magnetic field of 4.25 mG) and PKS 0637-752 (for magnetic fields of 6.5 and 9 mG) are comparable to their Eddington luminosities. Hence, it is possible that proton synchrotron emission could be the underlying mechanism of X-ray emission from their extended jets. Located at a redshift of 2.5, B3 0727+409 has a black hole mass of $3.3 \times 10^8\ M_\odot$

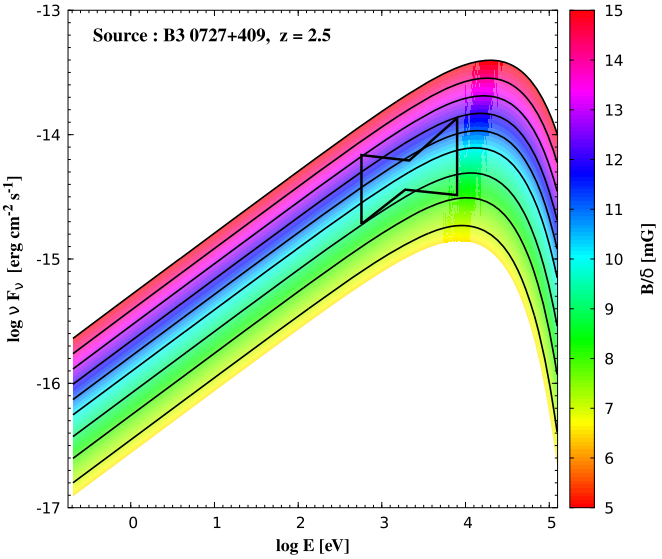

Figure 7. Same as Figure 5, but for the source B3 0727+409. The contour lines range from $\frac{B}{\delta} = 7$ to 15 mG in steps of 1 mG.

(Jamrozy et al. 2014) and an Eddington luminosity of 4×10^{46} erg s^{-1}. In Figure 7, the butterfly shows the possible X-ray emission from the extended jet of this source. In this case, the jet power required to explain the X-ray emission with a proton synchrotron model is 7.1×10^{48} erg s^{-1} (corresponding 10 mG), which exceeds the Eddington luminosity of this source.

We note that, due to the VHE gamma-ray emission of AP Librae, it is extremely difficult to model this source assuming equipartition in energy between the magnetic field and protons after maintaining all the relevant constraints. If we lower the magnetic field (at the expense of increasing the energy density of protons) to satisfy equipartition, we find that the Hillas criterion can no longer be maintained for the maximum proton energies required by the model. When the radius of the emission region is increased to satisfy the Hillas criterion at equipartition, the generated spectra overshoot the observed spectra by a significant amount, thus necessitating a departure from equipartition to successfully explain the observed SED. Also, a decrease in the magnetic field results in a significant increment of the maximum proton energy, which is already extremely high (3.98×10^{21} eV) and in tension with the maximum energies predicted by the theoretical models. Thus, it is evident that the SED of AP Librae cannot be modeled assuming equipartition; by contrast, because the sources 3C 279, PKS 0637-752, and B3 0727+409 are not detected in the VHE regime, they could be easily modeled with equipartition. The estimates of jet power obtained from the study presented in Figures 5–7 may vary to a certain extent on departure from equipartition, but nevertheless they still provide reasonable benchmarks for the acceptable range of the required jet power to model the SEDs.

The large-scale poloidal and toroidal magnetic fields in magnetohydrodynamic (MHD) jets have been studied (Vlahakis & Königl 2004; Komissarov et al. 2007; Romero et al. 2017). If magnetic flux is conserved in conical jets, then magnetic energy density decreases as the jet expands. In this case, if the magnetic field is purely poloidal it varies as $1/s^2$, and if it is purely toroidal it varies as $1/s$, where s is the distance from the black hole. But in the case of MHD-driven outflow, these relations are unlikely to remain valid. In our model also, the required magnetic fields in the blob, pc jet, and extended jet do not obey the s-dependence expected from conservation of magnetic flux, indicating the presence of MHD-driven outflow.

Here we note that, in earlier papers (Kundu & Gupta 2014 and Bhattacharyya & Gupta 2016), the luminosity required in the extended jet to explain the observed X-ray data was calculated by assuming a long jet lifetime of the order of 10^7–10^8 yr. After dividing the total energy required in the extended jet by the jet lifetime, the required luminosity was found to be lower than the Eddington luminosity.

4. Concluding Remarks

This paper discusses the possibility of applying the proton synchrotron model to the extended jet of AP Librae to explain the HE and VHE gamma-ray data. Our results indicate that, in order to successfully explain the VHE emission from the extended jet of AP Librae via proton synchrotron radiation, the following conditions are essential.

(i) The ambient magnetic field in the extended jet must be $\sim$1 mG.
(ii) Extremely HE protons $>10^{21}$ eV must exist in the extended jet.

Although the above conditions are consistent with the Hillas criterion, it is evident that the value of the ambient magnetic field required in the proton synchrotron model to explain the extended jet emission is at least an order of magnitude higher than that required in the IC/CMB model. We note that it would be possible to lower the magnetic field if we were to increase the value of Γ from the present value of 3. However, the jet power of the extended jet remains much higher than the Eddington luminosity of AP Librae. Thus, the proton synchrotron model is unlikely to explain the VHE gamma-ray emission from the extended jets of AGN.

The proton synchrotron model might explain the X-ray emission from the extended jets of some quasars, such as 3C 273 and PKS 0637-752. In future, with many more observations of extended X-ray jets, it will be possible to know whether IC/CMB and the proton synchrotron model are equally viable models for X-ray emission from extended jets.

We are thankful to Michael Zacharias and Stephen Wagner for providing us the data points used in Zacharias & Wagner (2016). We also gratefully acknowledge Ruo-Yu Liu and Felix Aharonian for critical reading of the manuscript and insightful comments. We also give our sincere gratitude to the anonymous referee for a detailed report on the manuscript which helped improve the paper significantly.

References

Abramowski, A. 2015, A&A, 573, 31
Aharonian, F. A. 2002, MNRAS, 332, 215
Aharonian, F. A., Belyanin, A. A., Derishev, E. V., et al. 2002, PhRvD, 66, 023005
Bhattacharyya, W., & Gupta, N. 2016, ApJ, 817, 121
Carini, M. T., Miller, H. R., Noble, J. C., & Sadun, A. C. 1991, AJ, 101, 1196
Cassaro, P., Stanghellini, C., Bondi, M., et al. 1999, A&AS, 139, 601
Cesarsky, C. 1992, NuPhB, 28, 51
Disney, M. J., Peterson, B. A., & Rodgers, A. W. 1974, ApJL, 194, L79
Ebisuzaki, T., & Tajima, T. 2014, APh, 56, 9
Franceschini, A., Rodighiero, G., & Vaccari, M. 2008, A&A, 487, 837
Henri, G., Pelletier, G., Petrucci, P. O., & Renaud, N. 1999, APh, 11, 347

Hervet, O., Boisson, C., & Sol, H. 2015, A&A, 578, 69
Hillas, A. M. 1984, ARA&A, 22, 425
Jamrozy, M., Stawarz, L., Marchenko, V., et al. 2014, MNRAS, 441, 1260
Kaufmann, S., Wagner, S. J., & Tibolla, O. 2013, ApJ, 776, 68
Komissarov, S. S., Barkov, M. V., Vlahakis, N., & Königl, A. 2007, MNRAS, 380, 51
Krawczynski, H., Hughes, S. B., & Horan, D. 2004, ApJ, 601, 151
Kühr, H., Witzel, A., Pauliny-Toth, I. I. K., & Nauber, U. 1981, A&AS, 45, 367
Kundu, E., & Gupta, N. 2014, MNRAS, 444, L16
Kusunose, M., & Takahara, F. 2017, ApJ, 835, 20
Lister, M. L., Aller, M. F., Aller, H. D., et al. 2013, AJ, 146, 120
Lucchini, M., Tavechhio, F., & Ghisellini, G. 2017, MNRAS, 466, 4299L
Miller, H. R., Clonts, S. L., & Folsom, G. H. 1974, AJ, 79, 1352
Paltani, S., & Türler, M. 2005, A&A, 435, 811
Petropoulou, M., Vasilopoulos, G., & Giannios, D. 2016, MNRAS, 464, 2213
Protheroe, R. J. 2002, PASA, 19, 486
Rachen, J. P., & Bierman, P. L. 1993, A&A, 272, 161
Romero, G. E., Boettcher, M., Markoff, S., et al. 2017, SSRv, 207, 5
Sanchez, D. A., Giebels, B., Fortin, P., et al. 2015, MNRAS, 454, 3229
Shakura, N. I., & Sunyaev, R. A. 1973, A&A, 24, 337
Vlahakis, N., & Königl, A. 2004, ApJ, 605, 656
Webb, J. R., Smith, A. G., Leacock, R. J., et al. 1988, AJ, 95, 374
Zacharias, M., & Wagner, S. J. 2016, A&A, 588, A110